Electrochemical oxidation of glucose in alkaline environment - A comparative study of Ni and Au electrodes

Alejandra Medrano-Banda, Erwann Ginoux, Théo Faverge, Alexandr Oshchepkov, Antoine Bonnefont, Marian Chatenet, Christophe Coutanceau, Gwénaëlle Kéranguéven, Patrick Cognet, Elena Savinova

Electrochimica Acta 487 (2024) 144159

Contents lists available at ScienceDirect

Electrochimica Acta

journal homepage: www.journals.elsevier.com/electrochimica-acta

Electrochemical oxidation of glucose in alkaline environment—A comparative study of Ni and Au electrodes

Alejandra Medrano-Banda [a], Erwann Ginoux [b,c], Théo Faverge [c,d], Alexandr Oshchepkov [a], Antoine Bonnefont [d], Marian Chatenet [d,*], Christophe Coutanceau [c], Gwénaëlle Kéranguéven [a], Patrick Cognet [b], Elena Savinova [a,*]

[a] ICPEES, UMR 7515 CNRS-University of Strasbourg, 25 rue Becquerel 67087 Strasbourg Cedex 2, France
[b] LGC, UMR 5503 CNRS-INP-ENSIACET, 4 allée Emile Monso, 31432 Toulouse Cedex 4, France
[c] IC2MP, UMR 7285 CNRS-University of Poitiers, 4 rue Michel Brunet, TSA 51106, 86073 Cedex 9 Poitiers, France
[d] LEPMI, UMR 5279 CNRS-University Grenoble Alpes, University Savoie Mont Blanc, 1130 Rue de la Piscine, 38610 Gières, France

ARTICLE INFO

Keywords:
Glucose oxidation reaction (GOR)
Nickel hydroxide
Gold
In situ Fourier Transform Infrared Spectroscopy (FTIRS)
Differential Electrochemical Mass Spectrometry (DEMS)
High Performance Liquid Chromatography (HPLC)

ABSTRACT

The glucose oxidation reaction (GOR) was studied on Au and Ni electrodes by cyclic voltammetry (CV), rotating disk electrode (RDE) measurements coupled with Koutecky–Levich analysis, Differential Electrochemical Mass Spectrometry (DEMS), *in situ* Fourier Transform Infrared spectroscopy (FTIRS) and High Performance Liquid Chromatography (HPLC) analysis of the reaction products after electrolysis in potentiostatic mode under continuous flow conditions. This study allowed to identify the reaction products and propose tentative reaction mechanisms. On gold, glucose is adsorbed on metallic sites through its anomeric function (C1) resulting in the formation of gluconate as the main GOR product at potentials close to 0.6 V *vs*. RHE, with a selectivity towards gluconate close to 100% and a projected faradaic efficiency of ca. 70%. The conversion rate is rather low, close to 20%, due to poisoning of the surface, leading to a strong deactivation. At potentials above 0.7 V *vs*. RHE, the selectivity towards gluconate decreases and non-selective GOR oxidation proceeds through C–C bond cleavage. On nickel, the GOR occurs at high potentials (close to 1.2 V *vs*. RHE) on $Ni(OH)_2$ and NiOOH sites, and proceeds through C1–C2 bond breaking, resulting in arabinose and formate. At higher potentials, the selectivity towards arabinose decreases, formate being the main reaction product.

1. Introduction

The electrocatalytic conversion of glucose has been broadly studied in the past, owing to its possible application in biosensors [1], synthesis of value-added products from biomass [2], fuel cells [3], and electrolyzers [4]. However, it is well known that the glucose oxidation reaction (GOR) can proceed in multiple oxidation steps and, therefore, the development of highly active, selective and stable electrocatalysts becomes crucial for its further implementation at large industrial scales. Several materials such as metals, metal oxides, alloys, complexes and carbon derivatives have been used to electrocatalyze the GOR in alkaline media; however, the first two groups remain the most studied and are usually used as models to understand this reaction [5]. Within the metals used for the GOR, platinum [6], palladium [7] and gold [8] electrodes have attracted particular interest, due to the low potentials at which they start to catalyze the reaction (<0.6 V *vs*. RHE) and high activity, with Au electrodes showing the highest selectivity (under certain conditions) towards value-added products such as gluconate [9]. On the other hand, the use of inexpensive earth-abundant materials such as cobalt [10], nickel [11,12] and copper [13] (hydr)oxides is considerably attractive, even though on these electrodes glucose is oxidized at higher potentials (>1.1 V *vs*. RHE). $Ni(OH)_2$ is particularly interesting, because of its high sensitivity towards glucose, which is of interest for sensor applications [14]. In practice, both Au and $Ni(OH)_2$ are representative materials that have been widely used for the study of the glucose oxidation reaction; however, the exact mechanism of oxidation is still elusive for both surfaces.

The generally accepted mechanism of glucose oxidation on Au in alkaline media involves the adsorption of glucose through the anomeric function and its subsequent electrochemical reaction, involving hydroxide species from solution for the formation of gluconate as a product [8]. Recent studies from Faverge et al. [15] and Neha et al. [9] have shown through cyclic voltammetry (CV), differential electrochemical mass spectrometry (DEMS) and *in situ* Fourier transform infrared spectroscopy (FTIRS), that GOR in the low potential region (<0.9 V *vs*.

* Corresponding authors.
E-mail addresses: marian.chatenet@grenoble-inp.fr (M. Chatenet), elena.savinova@unistra.fr (E. Savinova).

https://doi.org/10.1016/j.electacta.2024.144159
Received 26 January 2024; Received in revised form 22 March 2024; Accepted 24 March 2024
Available online 25 March 2024

RHE) proceeds through the adsorption of glucose on metallic Au sites and its subsequent reaction with either OH adsorbed on the surface, Au-OH, or OH^- from the electrolyte for the formation of gluconate and water. This agrees with studies made by Holade et al. where, through *in situ* FTIRS, the only product of GOR on Au/C electrodes was gluconate (at 0.5 and 0.8 V *vs*. RHE) [16]. However, recently, Schlegel et al. have detected gluconic acid and glucaric acid as the main products of the GOR on polycrystalline Au electrodes by high performance liquid chromatography (HPLC) at 0.55, 0.8 and 1.1 V *vs*. RHE, and suggested that glucose is first oxidized to gluconic acid, the latter being then oxidized to glucuronic acid and then to glucaric acid, transferring 2 e^- per each of these steps [17]. This selected literature review demonstrates that the mechanism, the nature of intermediates and products remain uncertain despite the large number of studies dedicated to the GOR on Au.

Contrary to Au, the oxidation of glucose on Ni is known to occur at high potentials (>1.1 V *vs*. RHE) through an electrochemical-chemical catalytic mechanism (EC′) in which $Ni(OH)_2$ is firstly electrooxidized to NiOOH, the latter reacting chemically with glucose to form an intermediate/product, and regenerate the $Ni(OH)_2$ species [18]. Even though this mechanism is generally accepted, it remains oversimplified and fails to fully describe the active sites involved in the reaction. Recently Danaee et al. studied the GOR on electrodeposited Ni/GC, and concluded that glucose requires the adsorption on NiOOH sites in order to react [19]. Contrariwise, Medrano-Banda et al. recently presented arguments in favor of glucose adsorption on the $Ni(OH)_2$ (rather than NiOOH) sites [20]. Furthermore, while gluconate was previously assumed the major product of the GOR on Ni [21], the study by Medrano-Banda et al. instead demonstrated generation of formate by *in situ* FTIRS on a Ni disk [20]. Moreover, Sanghez de Luna et al. performed GOR on Ni/NiO foams and detected a wide variety of products, including gluconic acid, glucaric acid, formic acid, arabinose, glycolic acid and tartronic acid by HPLC [22]. The variety of products observed suggests that the oxidation of glucose on Ni proceeds through the breaking of C–C bonds, which would hint at a more complex mechanism than the ones proposed previously and urges further efforts to understand the mechanism of the GOR on Ni.

From the above, it appears that different materials, metals or metal oxides, lead to completely different activity, stability, and products during electrochemical glucose oxidation. It is evident that a deeper understanding of the reaction mechanisms of the GOR on Au and Ni is necessary to design the next generation of active and selective electrocatalysts. For this reason, a comparative study of both Au and Ni electrodes for the GOR was performed by CV, rotating disk electrode (RDE), DEMS, *in situ* FTIRS and HPLC, to unveil the nature of the active sites, the products formed and the mechanisms through which this reaction occurs on different surfaces.

2. Experimental

2.1. Chemicals

All solutions were prepared using ultra-pure water with resistivity of 18.2 MΩ cm and <1 ppb TOC (PURELAB Chorus 1 or Millipore). HPLC grade water (Milli-Q system, Millipore) was used for all HPLC related measurements. The reagents $NiSO_4{\cdot}6H_2O$ (99.99%), $(NH_4)_2SO_4$ (99.0%), D-glucose (>99%), gluconic acid potassium salt (99%), D-fructose (99%), tartronic acid (97%), glycolic acid (99%), oxalic acid (98%), D-arabinose (>99%), sodium carbonate anhydrous (99.8%) and DL-glyceric acid hemicalcium salt hydrate (>98%) were purchased from Sigma Aldrich. Other reactants used were sodium bicarbonate (99.7%, ChemLab), formic acid (98%, Fisher Scientific), potassium hydroxide pellets (85%, Honeywell) and sulfuric acid (>95%–97%) (HPLC, Merck Millipore). All chemicals mentioned were used as purchased and without any further purification. NaOH (50% in water, Aldrich) was used either as-received or after Fe-purification, carried out according to the protocol inspired by Trotochaud et al. [23] and specified in Supplementary Information 1.1.

2.2. RDE measurements

The procedure used for the preparation of the bulk polycrystalline Au electrode (2 mm diameter) as well as the electrochemical setup used for measurements are described in detail elsewhere [15]. Ni_{ED}/GC and Ni_{ED}/XC72 samples were prepared by Ni electrodeposition on a 5 mm diameter glassy carbon (GC) electrode (the pretreatment of the GC electrode and Ni_{ED}/GC preparation are described elsewhere [20]). For Ni_{ED}/XC72, Vulcan XC-72 carbon (Cabot) was used as catalyst support with a loading of 100 μg cm^{-2}_{geom}. Electrodeposition of Ni on XC72 was performed at 25 °C from the N_2-saturated 0.01 M $NiSO_4$ and 0.1 M $(NH_4)_2SO_4$ solution in a glass cell with separate compartments for working (GC disk), counter (Ni wire), and reference ($Hg|Hg_2SO_4|K_2SO_4$ (sat.), MSE) electrodes. Electrodeposition was made under potentiostatic regime with rotation set at 400 rpm, with single step ($E = -1.45$ V *vs*. MSE with 150 mC charge transferred) deposition. After electrodeposition, Ni_{ED}/GC and Ni_{ED}/XC72 were quickly washed and transferred to the three-electrode Teflon cell. First, CVs were acquired in 0.1 M NaOH, without glucose. Then, a solution of 0.5 M glucose dissolved in 0.1 M NaOH was added to the electrochemical cell in a step-wise manner to reach the target concentration. The electrochemical set-up and parameters are explained elsewhere [20].

2.3. DEMS measurements

Mass spectrometry was coupled to cyclic voltammetry using a 50 nm thick metal film, sputtered onto a PTFE membrane (Cobetter PF-002H, 20 μm thickness, 20 nm pore diameter) as working electrode. The species probed were H_2, O_2 and CO_2 (m/z = 2, 32 and 44 respectively). CO (m/z = 28) was also detected, but it is considered as a fragment from CO_2. The detailed electrochemical and mass spectrometry setup is described elsewhere [15].

2.4. FTIRS measurements

Spectroelectrochemical measurements were performed at room temperature with a Bruker Vertex 80v Fourier transform infrared spectrometer equipped with a MCT (HgCdTe) detector cooled with liquid nitrogen. The GOR on Ni or Au bulk electrodes (10 and 9 mm diameter, respectively) was performed in a N_2 saturated Fe-unpurified 0.1 M NaOH solution using a glass cell with a ZnSe prism. A Pt wire and a Hg|HgO in 0.1 M NaOH (E = 0.94 V *vs*. RHE) electrodes were used as counter and reference electrodes, respectively. The spectra were collected in a double-sided acquisition mode between 700 and 4000 cm^{-1} with a resolution of 1 cm^{-1}. In order to obtain a single-beam spectrum, 64 interferograms were co-added and then Fourier transformed. The measurement protocol in potentiostatic mode was inspired by the work of Oshchepkov et al. [24] and consists of the following steps:

(i) First, the Ni disk electrode was submitted to 1.55 V *vs*. RHE for 30 min to grow $Ni(OH)_2$/NiOOH surface layer until the stabilization of current when cycling in the 0.93 to 1.6 V *vs*. RHE region. On Au disk several CVs were measured in the 0 to 1.5 V *vs*. RHE region until stabilization.

(ii) Then, glucose was injected to the cell to reach the target concentration of 5 mM (for Ni) or 25 mM (for Au) and a CV was recorded in the same potential interval.

(iii) Next, an initial potential (of 1.0 or 0.1 V *vs*. RHE for Ni and Au, respectively) was applied to the working electrode, at which it was pressed onto the prism and a background spectrum was recorded.

(iv) Finally, the electrode was polarized at the potentials of interest at which a series of FTIR spectra (typically 8) was collected in order to see the dynamics of their evolution with time.

All spectra of the reference compounds (glucose, gluconic acid, arabinose, oxalic acid, glycolic acid, formic acid, sodium bicarbonate and sodium carbonate) were recorded in ATR configuration using a hemispherical ZnSe prism and 256 interferograms with 1 cm^{-1} resolution.

2.5. HPLC measurements

Electrolysis measurements were conducted using a Micro Flow Cell supplied by ElectroCell, with a dedicated setup detailed in Supporting Information, Fig. 1 SI. 1.2. The electrodes used were either Ni foam or 'Au foam' acquired from Recemat BV, each having a geometrical surface area of 10 cm^2 (dimensions of 40 × 44 × 1.6 mm with only 10 cm^2 active area). The 'Au foam' was obtained by depositing a thick layer (2–3 μm) of Au on a Ni foam to ensure the absence of the signal from Ni and its influence on the performance. The reference electrode, a Ag|AgCl in 3.4 M KCl with a PEEK shaft, was placed within the cathode compartment for Ni foam experiments and within the anode compartment for Au foam experiments. Separation between the anodic and cathodic compartments was achieved using an anionic exchange membrane AHA from Eurodia. To maintain consistent flow rates in each compartment, two peristaltic pumps from Masterflex were employed, while the feeding solutions were continuously stirred using two magnetic stirrers from Cole-Parmer. 5 h electrolysis was realized and the current was measured at constant working electrode potential with a Radiometer potentiostat PGP201 controlled by a computer running VoltaMaster 4 software.

Following the electrolysis process, the samples were acidified by adding H_2SO_4 to achieve a pH in the range between 1 to 3 (pH 13 was initially measured for the electrolytes circulating in both cathodic and anodic compartments). The analysis was performed using a Thermo Vanquish HPLC system featuring a Vanquish Split Sampler and an Aminex HPX-87H column (300 mm × 7.8 mm, 9 μm particle size, 8% cross-linkage, pH range 1–3). Both ultraviolet (UV) and refractive index (RI) detectors were employed to detect reactants and products: a Vanquish Variable Wavelength UV detector capable of acquiring up to 4 wavelengths simultaneously, analyzing at a wavelength of 210 nm, and a RI detector RefractoMax 520. A mobile phase of 10 mM sulfuric acid was utilized under isocratic conditions, maintaining a flow rate of 0.6 mL min^{-1}. The injection volume was 20 μL, and the column temperature was maintained at 50 °C. The separation process required approximately 16 min. Quantification of the samples was carried out through external calibration curves (made of 5 independently prepared repetitions) over specific concentration ranges: 0.2 to 2 g L^{-1} for glucose, gluconic acid, sorbitol, fructose, and arabinose, and 0.01 to 1 g L^{-1} for formic acid, glycolic acid, oxalic acid, tartronic acid, and glyceric acid. Notably, all calibration curves exhibited a minimum regression coefficient (R^2) of 0.998, ensuring high precision and reliability for both the UV and RI detectors. For glucose and sorbitol, which were undetectable using the UV detector, the calibration curve was made from the RI detector only. The conversion (X), product selectivities (S) and faradaic efficiency (FE) were calculated following the equations detailed in Supporting Information (Eq. 1, 2 and 3 of SI. 1.3, respectively). A reminder of the molecular structures of the investigated products is available in Supporting Information 1.4, Fig. SI. 2.

3. Results and discussion

The experimental results obtained by cyclic voltammetry, RDE voltammetry coupled with Koutecky–Levich analysis, differential electrochemical mass spectrometry, *in situ* Fourier transform infrared spectroscopy and high-performance liquid chromatography after electrolysis are presented and discussed hereinafter.

3.1. Cyclic voltammetry

Cyclic voltammograms of Au and Ni electrodes acquired at low (10 mV s^{-1}) and high (100 mV s^{-1}) scan rate and shown in Fig. 1 demonstrate significant differences between the two metals. While on the Au surface, the GOR starts at potentials above ca. 0.3 V *vs*. RHE, that is in the potential interval where the Au surface is metallic, on Ni the GOR only occurs in the high potential interval, at ca. 1.2 V *vs*. RHE, that is ~100 mV before the onset of the $Ni(OH)_2$/NiOOH peak, as already observed for the oxidation of polyols [25]. Thus, on Ni the GOR is catalyzed by the $Ni(OH)_2$/NiOOH film, while on Au it is catalyzed by metal sites, formation of the oxide film above ca. 1.2 V *vs*. RHE resulting in surface passivation and decline of the catalytic activity. During the backward scan, the Au electrode reactivates as soon as the surface oxides are reduced. The shape of the CVs is also very different. For Au, the first low-potential wave is followed by two high-potential ones at 0.8 and 1.0 V *vs*. RHE, suggesting that the GOR mechanism and likely the reaction products depend on the electrode potential.

It is also instructive to compare the reactivity of gluconate, the prospective glucose oxidation product on Au, on the two electrodes. The CVs obtained on Au and on Ni in presence of gluconate (Fig. SI. 3) also demonstrate significant differences between the two metals. Indeed, CVs of the Au electrode in the presence of gluconate show no significant current until ca. 0.7 V *vs*. RHE, that is ca. 0.4 V above the 'onset' of the glucose oxidation, thus indicating that if glucose, in the potential interval from 0.3 to 0.7 V *vs*. RHE, is oxidized to gluconate, as suggested in previous publications [15], the latter will be a stable reaction product. On the contrary, on Ni the 'onset' of the gluconate oxidation is even lower than that of the GOR, which evidences that Ni cannot catalyze selective GOR into gluconate. At potentials higher than 0.7 V *vs*. RHE, gluconate on Au can be further oxidized (Fig. SI. 3) possibly into glucaric acid [17].

Thus, already the cyclic voltammetry measurements allow us to conclude that Au and Ni significantly differ in terms of the nature of the active sites and likely also the nature of the products.

3.2. Rotating disk electrode measurements

The RDE measurements at various rotation rate, from 100 to 2500 rpm followed by Koutecky–Levich (KL) analysis were conducted for Au and Ni electrodes (Fig. 2) in order to estimate the number of transferred electrons and their possible dependence on the electrode potential. The curves measured at 0 rpm are shown for comparison but were not used in the KL analysis. For Au, the measurements performed on a polycrystalline Au electrode and CVs acquired at different rotation rates demonstrated (Fig. 2a) an increase of the current, as expected for a mass-transport limited process. On the contrary, for the Ni_{ED}/GC electrode, currents were almost independent on the rotation rate (Fig. SI. 4a), suggesting that they are limited by reaction kinetics rather than by mass-transport. In order to shift the process into the mass-transport controlled regime, we prepared a Ni_{ED}/XC72 electrode with a high ECSA Ni electrode by electrodepositing Ni nanoparticles on a thin film of Vulcan XC-72 carbon immobilized on a GC disk. This, indeed, allowed us to observe the influence of the rotation rate on the currents (Fig. 2b).

The number of exchanged electrons can be estimated from KL analysis of voltammograms under steady-state conditions. On Au, these conditions are reached in the potential interval from 0.6 to 1.18 V *vs*. RHE. At higher potentials, the KL analysis is no longer relevant, due to the electrode deactivation and then the loss of stationary conditions. The number of electrons was determined using a glucose diffusion coefficient value of 6.70 × 10^{-6} cm^2/s and a kinematic viscosity value of 1.20 × 10^{-2} cm^2/s [26] as reported in Table 1.

One may see that at 0.6 V *vs*. RHE the number of electrons is comprised between 1 and 2, but increases with potential, suggesting that at high potential glucose undergoes consecutive oxidation steps. The influence of the potential on the GOR mechanism will be discussed hereinafter. At potentials above 1.0 V *vs*. RHE, the reader must consider the values into brackets as indicative only.

On Ni_{ED}/XC72, the GOR and the $Ni(OH)_2$/NiOOH transition are concomitant, therefore the catalyst surface is changing in parallel to the GOR, and no steady-state conditions are reached. Thus, KL analysis cannot be used to determine the number of exchanged electrons, as discussed in the Supporting Information (SI. 3).

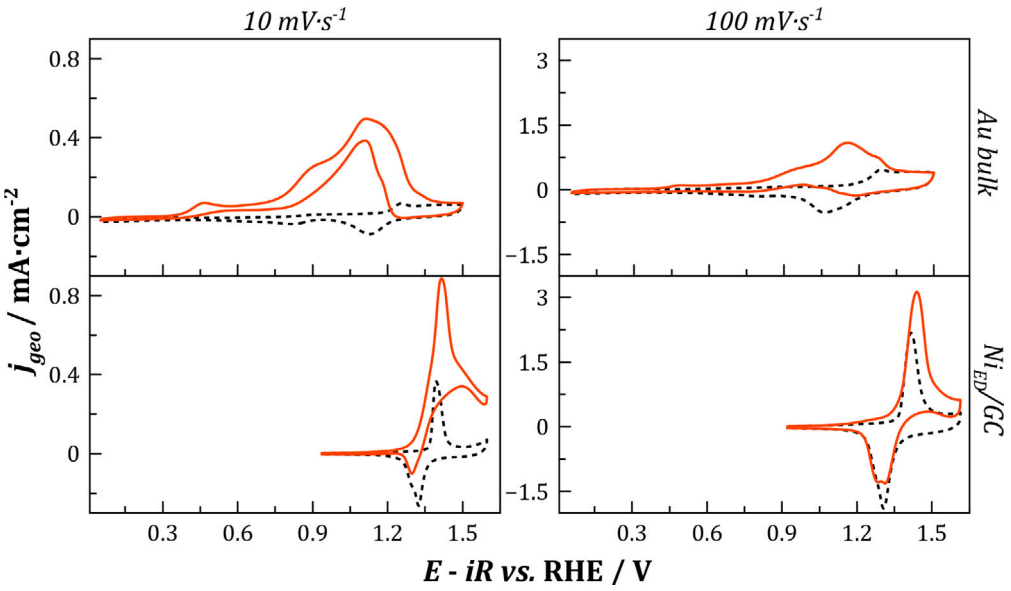

Fig. 1. CVs on bulk Au (top) and Ni_{ED}/GC (bottom) in N_2 purged 0.1 M NaOH with absence (black dotted line) and presence (red line) of 1 mM glucose at room temperature and measured at 10 (left) and 100 (right) mV s^{-1}. The electrochemical surface area (ECSA) for Au bulk and Ni_{ED}/GC was 0.1 and 0.6 cm^2, respectively.

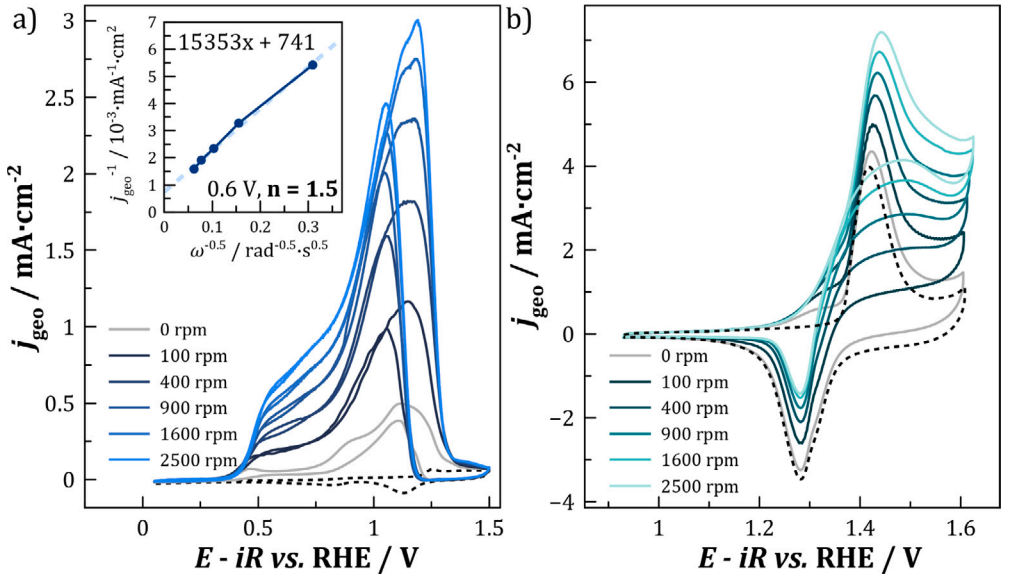

Fig. 2. Rotating disk CVs on (a) bulk Au and (b) Ni_{ED}/XC72 in 0.1 M NaOH with absence (black dotted line) and presence (solid lines) of 1 mM glucose at 25 °C and measured at 10 mV s^{-1}. The insert at (a) corresponds to the Koutecky–Levich plot obtained at 0.6 V. The ECSA for Au bulk and Ni_{ED}/XC72 was 0.1 and 15.2 cm^2, respectively.

Table 1
Electron numbers exchanged in the GOR on polycrystalline Au.

E/V *vs.* RHE	e^- number
0.6	1.5
0.78	2.3
0.88	4.6
0.98	8.1
1.08	(10.0)
1.18	(10.0)

3.3. Differential electrochemical mass spectrometry

The DEMS measurements (Fig. 3) showed that on gold, molecular hydrogen is released between 0.3 and 0.8 V *vs.* RHE, while no such signal could be detected on nickel, at any potential. The potential region in which H_2 is released on gold matches with the "plateau" region observed in the RDE experiment, in which the KL study allowed to propose a mechanism involving 1.5 e^- (close to 0.6 V) per glucose molecule. It is then coherent with the previously proposed mechanism [15], in which glucose dissociatively adsorbs onto the surface through C–H bond cleavage, leading to the formation of H_{ad} species. The glucose adsorbate can be oxidized through a 1 electron mechanism, and the H_{ad} species can either recombine to form H_2 through a Tafel step (chemical step, hence no additional electron transfer) or be oxidized in a Volmer step (1 additional electron transfer) leading to an overall transfer of 1 to 2 electrons, depending on the relative contribution of either the Tafel or Volmer step.

Another product detected on gold at potentials above 1.1–1.2 V *vs.* RHE is CO_2, which means that glucose is going through multiple oxidation steps, leading to C–C bond breaking and then CO_2. Again, this is coherent with the increasing number of electrons (up to 10) calculated for these high potentials through KL analysis. Interestingly, no CO_2

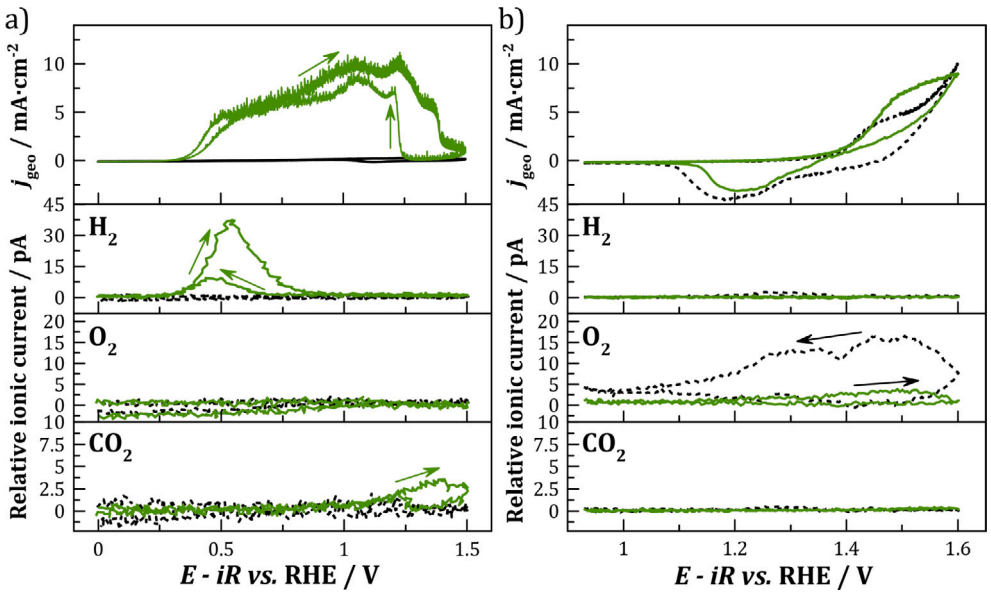

Fig. 3. DEMS measurements performed in CV mode on (a) Au and (b) Ni sputtered thin layer in 0.1 M NaOH aqueous solution in the absence (black dotted line) or presence (colored line) of 10 mM glucose, at 10 mV s^{-1} and at room temperature. The electrochemical current is reported in the top panels, while the relative ionic current of H_2, O_2 and CO_2 are reported in the bottom panels, as indicated.

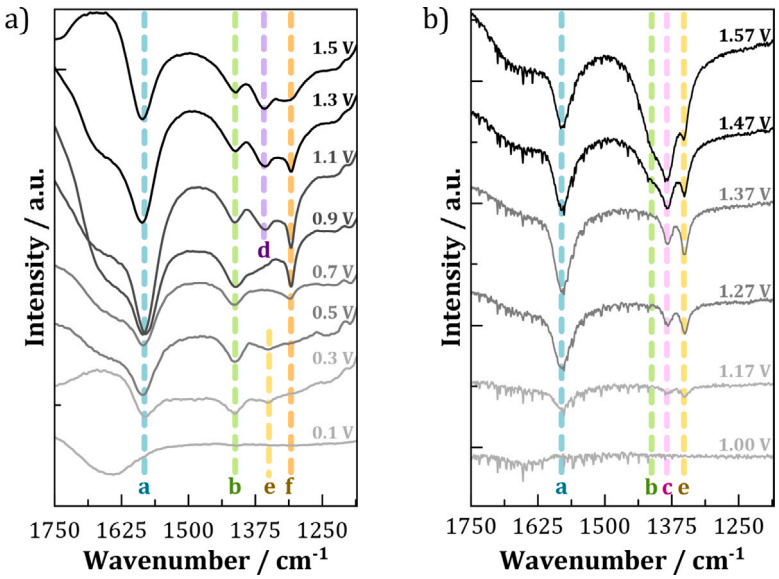

Fig. 4. FTIR spectra obtained during the GOR in 0.1 M NaOH measured at different potentials on either (a) a polycrystalline Au disk in the presence of 25 mM glucose, or (b) a polycrystalline Ni disk in the presence of 5 mM glucose. In (a) the spectra measured at 0.3 and 0.5 V were multiplied by a factor of 2 for clarity.

could be detected on the $Ni(OH)_2$ surface even at high potentials. This points again towards a very different GOR mechanism on Au and Ni.

Finally, at potentials higher than 1.5 V *vs*. RHE, O_2 production is evidenced on Ni in the blank electrolyte (0.1 M NaOH without glucose) on the forward scan. Observation of the oxygen signal on the backward scan, down to very low potentials, may be attributed to bubbles stuck in the pores of the sputtered Ni electrode. The addition of glucose into solution completely inhibits this oxygen production. This could be explained either by the GOR and OER competition, with GOR being favored in the potential interval of the OER, or surface blocking by glucose or its derivatives.

3.4. *In situ Fourier transform infrared spectroscopy*

FTIR spectra were measured on polycrystalline Au and Ni electrodes in the external reflection configuration. To minimize local effects (pH changes, depletion of glucose concentration, consecutive transformation of the GOR products), the measurements were performed in a sequence of potential steps, each step followed by lifting the electrode and re-establishing the thin-layer configuration. Fig. 4 shows the appearance of vibrational bands, which corresponds to the formation of the GOR products, being different in the case of Au and Ni electrodes.

On the Au electrode, the main bands start appearing around 0.3 V *vs*. RHE, which agrees with the electrochemical and DEMS data. Bands a and b at 1580 and 1415 cm^{-1} (corresponding to the asymmetric and symmetric stretching of the carboxylate group), and e at 1350 cm^{-1} (corresponding to the bending of the methylene group) point towards the production of gluconate in the potential interval from 0.3 to 0.7 V *vs*. RHE (Table 2). As the electrode potential reaches 0.7 V *vs*. RHE, a new band (band f, 1310 cm^{-1}) appears, revealing the formation of oxalate species. This attribution agrees well with literature and internal references measured at the same pH, as shown in Fig. SI. 7. Finally,

Table 2
FTIRS band attribution.

Label	Wavenumber/cm^{-1}	Vibration	Proposed attributions	References
a	1580	ν_{asym}O–C–O	Carboxylate	[27]
b	1415	ν_{sym}O–C–O	Gluconate	[16]
c	1385	ν_{sym}O–C–O	Formate	[28]
d	1360	ν C–O	Carbonate/bicarbonate	[29]
e	1350	δ_{CH_2}	Carboxylate	[30]
f	1310	ν C–O	Oxalate	[31]

starting from ca. 0.9 and 1.3 V *vs*. RHE the bands at 1360 (band d) and 2343 cm^{-1} appear, respectively, suggesting the formation of carbonates and then dissolved CO_2 (Fig. SI. 6) in agreement with the DEMS data. This confirms that C–C bond breaking occurs during the GOR on Au at high potential.

On Ni, vibrational bands of the GOR products start appearing around 1.17 V *vs*. RHE. In agreement with the electrochemical data, no gluconate formation could be observed on Ni at potentials below 1.47 V *vs*. RHE, bands a, c and d rather pointing to production of formate, hence evidencing C–C bond breaking. Neither oxalate (band f) nor CO_2 were evidenced here, which is coherent with the DEMS data. It is then reasonable to propose that the carbon chain of glucose is oxidized differently on Au and Ni, as the oxidation products are different. Finally, at potentials higher than 1.47 V *vs*. RHE (that is in the potential interval where anodic current in the presence of gluconate drops, see Fig. SI. 3), the band b attributed to gluconate appears as a shoulder, suggesting formation of gluconate as a by-product. In the meantime, bands a, c and d keep increasing their intensity with potential.

While FTIRS in thin layer configuration is a relevant technique to observe *in situ* products formed depending on the potential applied, it is prone to local effects related to local pH changes, depletion of the reactant concentration, and consecutive transformation of the reaction products trapped in the thin layer. Furthermore, while infra-red spectroscopy is useful in identifying various functional groups (alcohol, carbonyl, carboxylic, etc.), it has limited utility in distinguishing molecules with similar functional groups, such as various carbohydrates. To aid in identification of various GOR products, an *ex situ* characterization technique such as HPLC can be used after electrolysis at constant potential.

3.5. High performance liquid chromatography

The products obtained after constant potential electrolysis in a continuous flow reactor at various potentials applied to either Au or Ni anode were determined by HPLC. Some of the chromatograms obtained are presented in Figs. 5 and 6 for Au and Ni correspondingly.

As expected, different products were identified upon electrolysis on Au and Ni electrodes. The results suggest that gluconate is the major product on gold, as expected. The conversion, selectivity towards gluconic acid, and faradaic efficiency were calculated for potentials between 0.6 and 1.28 V *vs*. RHE. Despite the results of the KL analysis point towards a number of electrons increasing with potential, calculations of the *FE* were performed assuming a one-electron process at any potential, as the gluconate production involves only one electron on Au. The additional electrons originate from H_{ad} oxidation in a Volmer step at low potentials, and then from the carbon chain oxidation, eventually until CO_2 production, as evidenced by the DEMS experiment. Note however that the complete oxidation of glucose into CO_2 following the reaction ($C_6H_{12}O_6 + 24OH^- \rightarrow 6CO_2 + 18H_2O + 24e^-$) should involve the transfer of 24 electrons, which is much higher than what was evaluated through the KL analysis. This indicates that the oxidation to CO_2 makes only a small contribution to the overall process. C–C bond breaking in glucose, along with CO_2 production, leads to the production of low amounts of other by-products, such as tartronic acid, glyceric acid, glycolic acid, formic acid and also oxalic acid. Some of these products were detected in amounts close or below the quantification limit. A part of them can be further oxidized into CO_2, not detectable by HPLC. Moreover, despite the electrolyte being continuously N_2-purged, some oxygen traces remain in the solution, leading to a non-negligible ORR current of ca. 7 mA at 0.6 V *vs*. RHE (see Fig. SI. 8) that overlaps with the GOR current. For these reasons, calculation of the *FE* should be considered as indicative only, the most relevant value being the selectivity. Results are synthesized in Table 3 and in Table SI. 4.

Table 3
Chemical conversion, selectivity and faradaic efficiency towards gluconic acid during the GOR on Au foam. At 0.6 V *vs*. RHE, the raw value (uncorrected from the ORR) of the *FE* would be 150%. An estimation of a corrected value is 70% *FE* at 0.6 V *vs*. RHE, see Fig. SI. 9. No correction were made on the *FE* values at higher potential.

E/V *vs*. RHE	0.6	0.78	0.88	0.98	1.08	1.18	1.28
X/ %	16.3	24.1	21.5	24.8	23.1	29.6	47.3
$S_{gluconic\ acid}$/ %	100	73.6	70.9	70.6	74	74.3	83.4
$FE_{gluconic\ acid}$/ %	70	62	51	50	44	38	41

Table 4
Electrolysis performances during GOR on Ni foam.

E/V *vs*. RHE	1.0	1.47	1.6
X/ %	2	5	5
$S_{arabinose}$/ %	–	45	64
$FE_{arabinose}$/ %	–	72	40
$S_{formic\ acid}$/ %	–	104	182
$FE_{formic\ acid}$/ %	–	117	92

The conversion rate increases from 16 to 47% with the increase of the applied potential. These rather low values after 5 h of electrolysis can be explained by a strong deactivation of the electrode, possibly due to the surface poisoning by adsorbates [32]. Cycling the electrode in the potential interval between 0 V *vs*. RHE and the originally applied potential allows to reactivate its surface as illustrated in Supporting Information (Fig. SI. 10). However, the calculations in the work were done without reactivation to ensure a more relevant comparison with electrolysis on Ni, where the reactivation was not performed.

The selectivity towards gluconic acid stays within the 70%–83% range, with no clear dependence on the applied potential, except for the electrolysis at 0.6 V *vs*. RHE where it reached 100%. The other products detected were tartronic acid, glyceric acid, glycolic acid, and formic acid with selectivities between 2 and 10% depending on the potential applied. In this context, it is worth mentioning that potentials could not be ohmic drop-corrected (since currents during the electrolysis decayed in time due to the poisoning resulting in time-dependent ohmic drop values) and thus the actual electrode potentials are lower than the applied ones, the electrolyte resistance was estimated to be around 5 Ω.

Finally, the *FE* (calculated assuming 1 e$^-$ transfer) decreases with the applied potential, from 70% at 0.6 V *vs*. RHE to only ca. 40% at 1.28 V *vs*. RHE. The latter likely arises from the formation of a mixture of products with different numbers of transferred electrons making the *FE* analysis ambiguous. Thus, to perform selective GOR into gluconate on Au, the applied potential should be set around 0.6 V *vs*. RHE.

For the Ni foam, the products obtained after a 1 h of potential-controlled electrolysis of a 27 mM glucose solution in a continuous flow reactor were also determined by HPLC. The chromatograms obtained are presented in Fig. 6, from where it is possible to observe that the main products differ significantly from those on Au. As discussed previously, little gluconate could be detected, the main products being arabinose (C5 sugar) and formic acid (C1 compound) [33], as summarized in Table 4 and in the Supporting Information, Table SI 5.

First, at 1.0 V *vs*. RHE no GOR current could be detected (Fig. SI. 11), nonetheless, a small decrease of the glucose concentration (the estimated conversion rate of 2%) and some GOR products (albeit

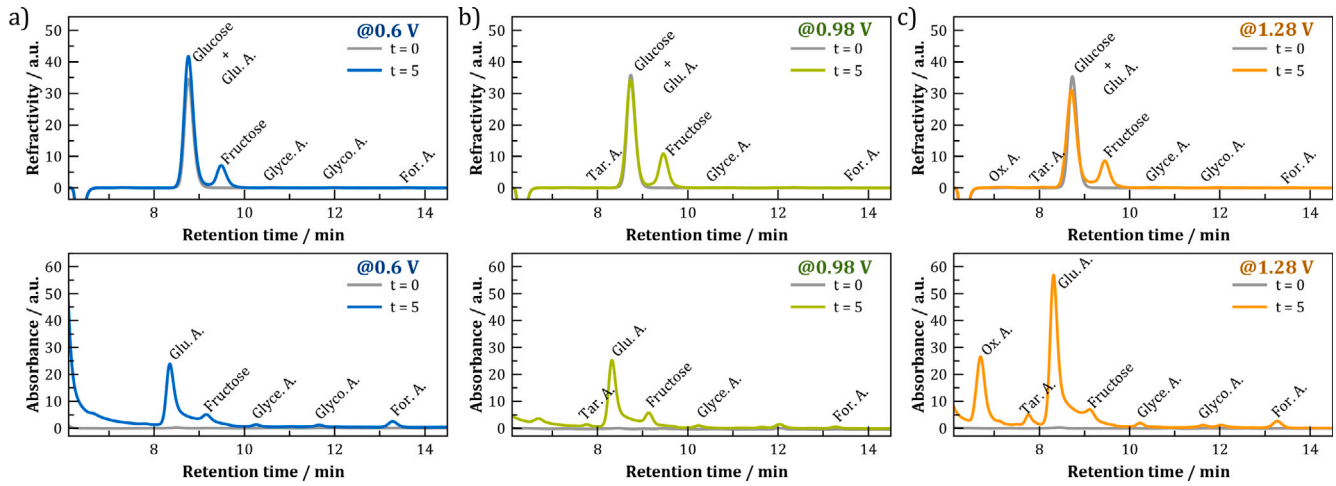

Fig. 5. Chromatograms measured before (gray line) and after (colored line) 5 h of electrolysis on Au foam in N_2 saturated 0.1 M KOH and 27 mM glucose at 0.6 (a, blue line), 0.98 (b, green line) and 1.28 (c, orange line) V *vs.* RHE. Two detectors were used: RI (top) and UV (bottom).

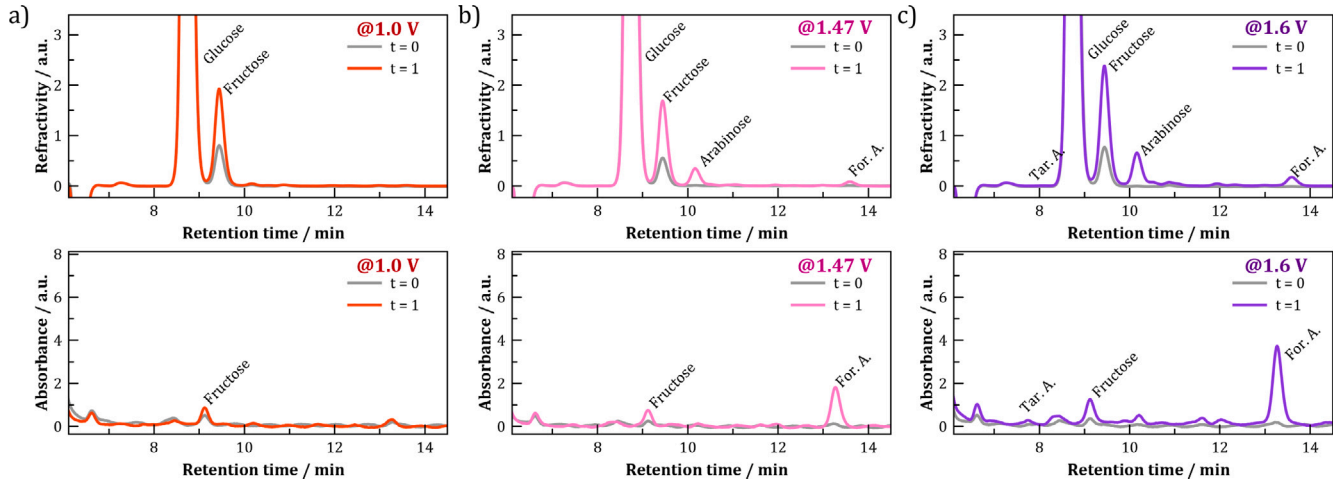

Fig. 6. Chromatograms measured before (gray line) and after (colored line) 1 h electrolysis on Ni foam in N_2 saturated 0.1 M KOH and 27 mM glucose at 1.0 (a, red line), 1.47 (b, pink line) and 1.6 (c, purple line) V *vs.* RHE. Two detectors were used: RI (top) and UV (bottom).

below the quantification limit) were observed and can be attributed to the degradation of glucose in alkaline media in the presence of oxygen traces (products of glucose degradation in presence of oxygen are presented in Table SI. 6). At potentials of 1.47 and 1.6 V *vs.* RHE, the conversion rate reached 5% after 1 h of electrolysis. As a C5 (arabinose) and C1 (formic acid) products are produced from a C6 compound (glucose), it is straightforward to suppose that Ni breaks the C–C bond to form those two species as fragments of the initial glucose molecule. However, the calculated selectivities for both products do not match each other: roughly two moles of formic acid were produced for one mole of arabinose at 1.47 V *vs.* RHE, while this ratio increases to 3:1 at 1.6 V *vs.* RHE. This is attributed to multiple uncontrolled oxidation steps occurring on Ni at high potentials. Thus, the calculated selectivities and faradaic efficiencies should be considered cautiously.

3.6. Glucose electrooxidation mechanism

The results obtained by cyclic voltammetry, Koutecky–Levich analysis, DEMS, FTIRS and HPLC suggest that the GOR on gold and nickel electrodes follows different reaction mechanisms. These differences could originate from different surface state and/or different surface charge of these electrodes, which will be analyzed in what follows.

On Au, the GOR starts at potentials (>0.3 V *vs.* RHE) at which the surface is metallic. According to the literature, Au is expected to be negatively charged in the potential interval of the GOR. Indeed, the potential of zero charge (E_{pzc}) depends on the surface crystallography [34] and for Au(111) is given on the RHE scale by E_{pzc} = 0.474 V + 0.059 pH [35], thus E_{pzc} = 1.24 V *vs.* RHE at pH 13. Considering the E_{pzc} value, results of DEMS and previous publications [9,15], we conclude that the first step of the GOR on Au is the dissociative adsorption of glucose (noted Glu-H) through its anomeric function onto a metallic site (noted Au), leading to the formation of glucose and hydrogen adsorbates (Glu_{ad} and H_{ad}, respectively). This corresponds to step 1 in the schematic representation of GOR mechanism on Au shown in Fig. 7.

$$Glu - H + 2\ Au \longrightarrow Glu_{ad} + H_{ad} \quad (1)$$

Formation of H_{ad} is supported by the release of molecular hydrogen (detected by DEMS experiments) resulting from recombination of hydrogen adatoms through a chemical recombination (Tafel) step (step 3 in Fig. 7) :

$$2\ H_{ad} \longrightarrow 2\ Au + H_2 \quad (2)$$

Dissociative adsorption of glucose is followed by the oxidation of the glucose adsorbate into gluconate ($C_6H_{11}O_7^-$, noted Gla^-) as evidenced by HPLC, through a one-electron process (steps 4 and 5 in Fig. 7).

$$Glu_{ad} + 2\ OH^- \longrightarrow Au + Gla^- + H_2O + 1\ e^- \quad (3)$$

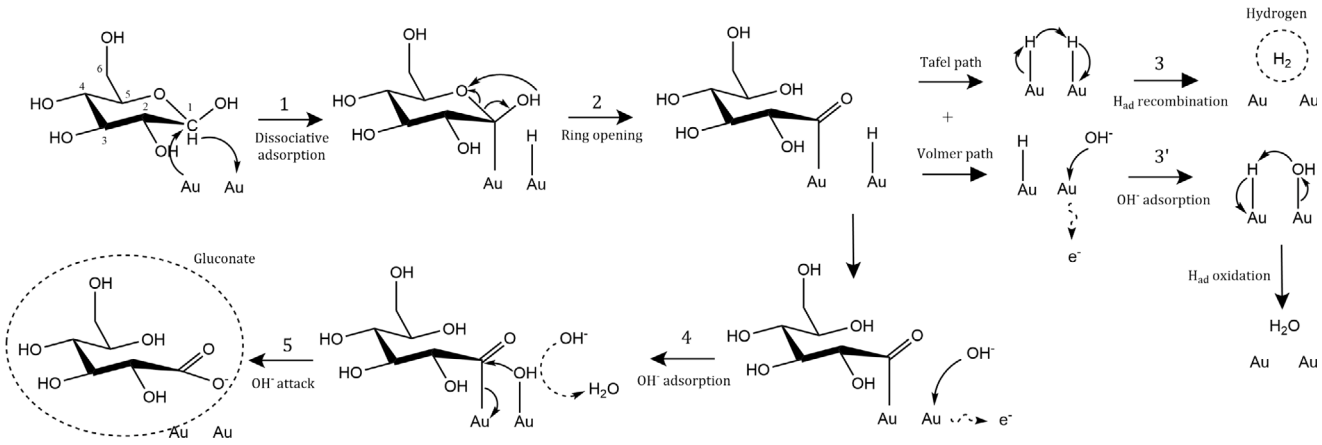

Fig. 7. Tentative mechanism of the GOR on Au surface for potentials below 0.7 V *vs.* RHE, leading to gluconate formation.

The GOR through Eqs. (1), (2) and (3) is a one-electron process, while, according to the KL analysis, at low potentials (close to 0.6 V *vs.* RHE), the average number of transferred electrons is 1.5. This can be explained by the hydrogen adatoms oxidation through a Volmer step (Eq. (4), step 3′ in Fig. 7) occurring in parallel to the Tafel step.

$$H_{ad} + OH^- -> Au + H_2O + 1\ e^- \quad (4)$$

With increasing potential, more and more glucose adsorbates are oxidized, leading to an increase of the surface coverage in H_{ad} species, and thus an increase in the contribution of the Tafel reaction (Eq. (2)). At higher potential, the direct oxidation of the H_{ad} species (Eq. (4)) becomes predominant, explaining the decrease of hydrogen signal measured by DEMS and the corresponding increase of number of electrons calculated through the KL analysis. An absence of a plateau in the RDE voltammograms at $E > 0.5$ V *vs.* RHE (Fig. 2) also reflects an increasing number of electrons transferred in the GOR. Note that specific hydroxide adsorption occurs on Au above ca. ~0.5 V *vs.* RHE (depending on the surface crystallography) [36,37] hinting that adsorbed OH species may start participating in the GOR mechanism (step 4 in Fig. 7).

At potentials higher than 0.7 V *vs.* RHE, one can observe a significant increase of the current measured on the CV, together with a number of exchanged electrons higher than 2. This agrees with the FTIRS data suggesting further oxidation of gluconate into oxalate (evidenced by HPLC at potentials around 1.28 V *vs.* RHE) in a thin layer configuration. At higher potentials, DEMS and FTIRS experiments evidenced the oxidation of carbon chain with CO_2 production, pointing to uncontrolled oxidation of the glucose through successive C–C bond breaking steps. Note that the residence time in the vicinity of the electrode surface and glucose over OH^- concentration ratio most likely have a strong influence on the oxidation path [17], and could be somewhat different under the conditions of FTIRS, DEMS, and HPLC measurements, complicating direct comparison under exactly the same potential. The GOR mechanism in the interval of high potentials is yet to be understood precisely.

On Ni, no current is observed in the presence of glucose below ~1.2 V *vs.* RHE (see Fig. 1), evidencing that the GOR occurs on $Ni(OH)_2$/NiOOH but not on metallic surface sites. A recent study by Medrano-Banda et al. [20] suggests that glucose is adsorbed on the $Ni(OH)_2$ sites and then reacts with the NiOOH sites, the latter formed above ~1.4 V *vs.* RHE through a one-electron $Ni(OH)_2$/NiOOH redox transition. The GOR 'onset' being much inferior than the 'onset' of the $Ni(OH)_2$/NiOOH transition peak suggests that either glucose reacts already on the $Ni(OH)_2$ sites, or, more likely, that the initial step of the $Ni(OH)_2$ into NiOOH transformation occurs below the peak 'onset', as previously suggested for the glycerol oxidation reaction [25,38,39]. Indeed, according to the ellipsometry study of Visscher [40], changes in the refractive index of a Ni electrode start already above ~1.17 V *vs.* RHE, that is exactly at the potential where FTIR spectra show the start of the product formation (Fig. 4).

Both HPLC and FTIRS data evidence that the GOR on $Ni(OH)_2$/NiOOH occurs through a C–C bond cleavage, contrary to Au, where it proceeds via oxidation of the anomeric into an acidic function, at least in the low potential interval. Previous studies suggest that, on $Ni(OH)_2$/NiOOH, mono-alcohols undergo selective electrooxidation of the alcohol into either aldehyde/ketone [41] or acidic function [42], while polyols (including carbohydrates) are prone to C–C bond breaking [43]. According to DFT calculations, C–C bond breaking in glycerol on NiOOH occurs through a bridge-bonded adsorbed intermediate [44].

We assume that glucose adsorption on $Ni(OH)_2$ sites occurs via C–O bond formation between negatively charged $Ni-O^-$ surface species and carbon atoms of the glucose molecule, as depicted in the schematic representation of the GOR mechanism on Ni, shown in Fig. 8. Indeed, even though the values of pzc and isoelectric point of Ni(II) oxides/hydroxides reported in the literature vary significantly (from 7.5 to 11.8, see [45,46]), in any case at pH 13, the surface of $Ni(OH)_2$ is expected to be negatively charged, exposing $Ni-O^-$ groups to the surface. This C–O bond formation is facilitated by the positive charge on carbon atoms, calculations suggesting the positive charge being confined on C1, C2, C4 and C5 glucose atoms [47]. Considering steric hindrance on C6, dissociative glucose adsorption is expected to occur through C1–C2 bond cleavage, which agrees with the formation of formic acid and arabinose. Increase of the formic acid/arabinose molar ratio with potential can be attributed to consecutive C–C bond breaking steps in arabinose.

At higher potentials, when the surface is fully NiOOH-covered, the mechanism is likely to change, involving glucose dissolved in the electrolyte reacting with surface NiOOH (see SI. 3.2 and Ref. [20]).

4. Conclusions

The glucose oxidation reaction was studied on Au and Ni electrodes. The two metals show grossly different electrocatalytic properties. On Au, it is the metal sites that are active in the GOR, formation of Au oxide/hydroxide passivating the surface and resulting in the loss of electrocatalytic activity. Combined evidence from electrochemistry, DEMS, FTIRS and HPLC indicate that glucose oxidation on Au starts at potentials above 0.3 V *vs.* RHE and results in its selective conversion into gluconate up to ca. 0.7 V *vs.* RHE, where gluconate can be further oxidized. Together with DEMS experiment, that evidences the production of molecular H_2 at potentials close to 0.6 *vs.* RHE, the Koutecky–Levich study made by RDE measurements allows to estimate that this oxidation into gluconate occurs with one electron exchanged for the oxidation of adsorbed glucose, and a second electron coming from the possible oxidation of the H_{ad} species. Thus, the overall electron number exchanged per glucose molecule is between 1 (all H_{ad}

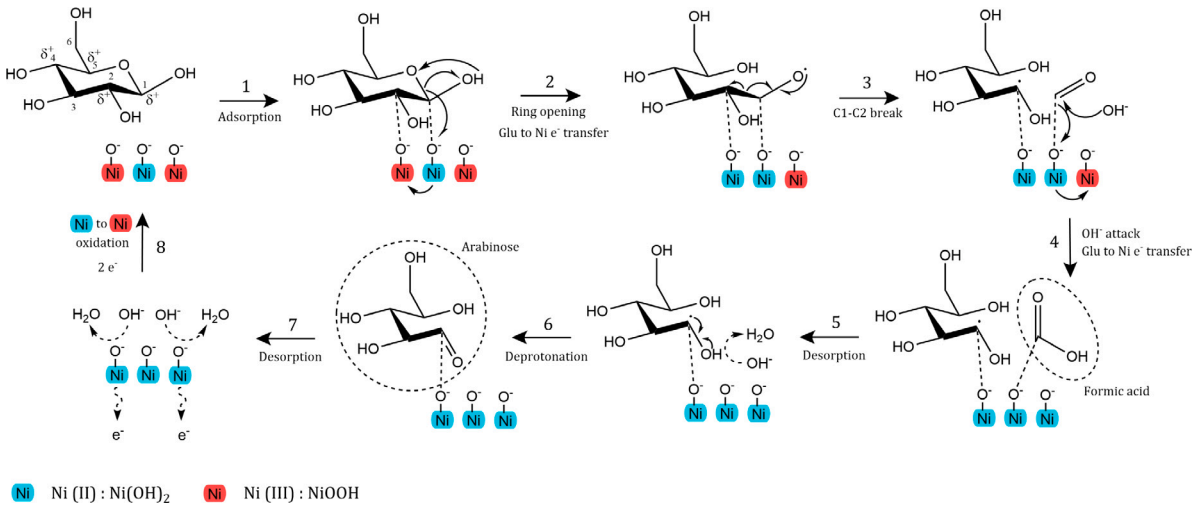

Fig. 8. Tentative mechanism of the GOR on $Ni(OH)_2$/NiOOH surface at potentials above 1.2 V *vs.* RHE, leading to arabinose and formic acid.

species recombining through Tafel step) and 2 (all H_{ad} species oxidized through Volmer step). At higher potential, up to 10 exchanged electrons were estimated by Koutecky–Levich study, and CO_2 production was evidenced by DEMS and FTIRS, indicating C–C bond cleavage and thus the loss of selectivity towards gluconate. Although only a rather low conversion rate (16 to 47%) could be achieved due to strong deactivation of the gold surface, HPLC measurements after 5 h electrolysis at constant potentials revealed that the selectivity towards gluconic acid reached 100% with a projected faradaic efficiency of 70% at 0.6 V *vs.* RHE. Cycling the electrode between the initial potential and 0 V *vs.* RHE is an easy and efficient way to reactivate the Au electrode, and thus reach higher conversion rates, while preserving the high selectivity towards gluconate.

On Ni, metallic surface sites are inactive in the GOR, the reaction beginning at potentials as high as ~1.2 V *vs.* RHE, where the electrode surface is covered by $Ni(OH)_2$. Besides, the oxidation of gluconate starts at a lower potential, suggesting that selective gluconate formation is not feasible on Ni. The different nature of the surface sites strongly impacts the GOR mechanism, the reaction occurring through C–C bond breaking (likely between C1 and C2 atom) and results in formic acid (C1 acid, detected by FTIRS and HPLC) and arabinose (C5 sugar, detected by HPLC). However, the molecular fractions of formic acid and arabinose are not the same, suggesting that glucose and/or arabinose molecules may be subject to multiple C–C bond breaking and oxidation steps. Contrary to the gold surface, DEMS evidenced no CO_2 formation, even at high electrode potentials. It has also been demonstrated that the presence of glucose completely inhibited the OER on Ni, either because of competing reaction mechanisms or because of surface blocking by glucose molecules. Experimental and simulation data demonstrated that the $Ni(OH)_2$/NiOOH surface is not under stationary conditions during the GOR, making Koutecky–Levich analysis of the rotation rate dependence inappropriate.

Further than the catalyst nature, parameters such as the residence time, poisoning, the glucose over hydroxide concentration ratio and the oxidation state of the surface seem to have a large influence on the glucose oxidation mechanism. Thus, a better understanding of the effect of these parameters on the stability, conversion rate, selectivity and faradaic efficiency is a prerequisite to the implementation of efficient electrolysers for biomass-derived compounds at an industrial scale.

CRediT authorship contribution statement

Alejandra Medrano-Banda: Writing – original draft, Investigation, Data curation. **Erwann Ginoux:** Writing – original draft, Investigation, Data curation. **Théo Faverge:** Writing – original draft, Investigation, Data curation. **Alexandr Oshchepkov:** Writing – review & editing, Investigation. **Antoine Bonnefont:** Writing – review & editing, Supervision, Conceptualization. **Marian Chatenet:** Writing – review & editing, Supervision, Conceptualization. **Christophe Coutanceau:** Writing – review & editing, Supervision, Conceptualization. **Gwénaëlle Kéranguéven:** Writing – review & editing, Supervision. **Patrick Cognet:** Supervision. **Elena Savinova:** Writing – review & editing, Supervision, Project administration, Funding acquisition, Conceptualization.

Declaration of competing interest

The authors declare that they have no known competing financial interests or personal relationships that could have appeared to influence the work reported in this paper.

Data availability

Data will be made available on request.

Acknowledgments

This study was funded by the French National Research Agency (ANR), France: grant ANR-20-CE43-0005. The authors acknowledge Bruno Gilles for the sputtered metal layers used in DEMS experiment.

Appendix A. Supplementary data

Supplementary material related to this article can be found online at https://doi.org/10.1016/j.electacta.2024.144159.

References

[1] J. Wang, Electrochemical glucose biosensors, Chem. Rev. 108 (2008) 814–825, http://dx.doi.org/10.1021/cr068123a.
[2] Z.I. Lai, L.Q. Lee, H. Li, Electroreforming of biomass for value-added products, Micromachines 12 (2021) 1405, http://dx.doi.org/10.3390/MI12111405.
[3] J. Chen, H. Zheng, J. Kang, F. Yang, Y. Cao, M. Xiang, An alkaline direct oxidation glucose fuel cell using three-dimensional structural Au/Ni-foam as catalytic electrodes, RSC Adv. 7 (2017) 3035–3042, http://dx.doi.org/10.1039/C6RA27586A.
[4] C. Lin, H. Li, P. Zhang, C. Deng, L. Meng, Q. Zhou, S. Wang, J. Wu, C. Liu, J. Tian, Y. Qian, Boosting water electrolysis with anodic glucose oxidation reaction over engineered cobalt nickel hydroxide nanosheet on carbon cloth, J. Electroanal. Soc. 861 (2020) 113946, http://dx.doi.org/10.1016/j.jelechem.2020.113946.
[5] K.E. Toghill, R.G. Compton, Electrochemical non-enzymatic glucose sensors: A perspective and an evaluation, Int. J. Electrochem. Sci. 5 (2010) 1246–1301, http://dx.doi.org/10.1016/S1452-3981(23)15359-4.

[6] M.F. de Mele, H.A. Videla, A.J. Arvía, The electrooxidation of glucose on platinum electrodes in buffered media, J. Electroanal. Chem. Interfacial Electrochem. 155 (1983) 239–249, http://dx.doi.org/10.1016/S0022-0728(83)80479-3.

[7] C.C. Hu, T.C. Wen, Voltammetric investigation of palladium oxides-II. Their formation / reduction behaviour during glucose oxidation in NaOH, Electrochim. Acta 39 (1994) 2763–2771, http://dx.doi.org/10.1016/0013-4686(94)00291-6.

[8] Y.B. Vassilyev, O.A. Khazova, N.N. Nikolaeva, Kinetics and mechanism of glucose electrooxidation on different electrode-catalysts: Part II. Effect of the nature of the electrode and the electrooxidation mechanism, J. Electroanal. Chem. Interfacial Electrochem. 196 (1985) 127–144, http://dx.doi.org/10.1016/0022-0728(85)85085-3.

[9] N. Neha, T. Rafaïdeen, T. Faverge, F. Maillard, M. Chatenet, C. Coutanceau, Revisited mechanisms for glucose electrooxidation at platinum and gold nanoparticles, Electrocatalysis 14 (2022) 121–130, http://dx.doi.org/10.1007/s12678-022-00774-y.

[10] J. Hu, H. Lu, M. Li, G. Xiao, M. Li, X. Xiang, Z. Lu, Y. Qiao, Cobalt valence modulating in CoO incorporated carbon nanofiber for enhanced glucose electrooxidation, Mater. Rep.: Energy 2 (2022) 100091, http://dx.doi.org/10.1016/j.matre.2022.100091.

[11] M. Fleischmann, K. Korinek, D. Pletcher, The oxidation of organic compounds at a nickel anode in alkaline solution, J. Electroanal. Chem. Interfacial Electrochem. 31 (1971) 39–49, http://dx.doi.org/10.1016/S0022-0728(71)80040-2.

[12] A.M. Abdelrahim, M.G. Abd El-Moghny, M.E. El-Shakre, M.S. El-Deab, Promoted glucose electrooxidation at $Ni(OH)_2$/graphene layers exfoliated facilely from carbon waste material, RSC Adv. 13 (2023) 1811–1822, http://dx.doi.org/10.1039/D2RA07309A.

[13] A.H. Dourado, A.G. da Silva, F.A. Pastrián, R.L. Munhos, A.P. de Lima Batista, A.G. de Oliveira-Filho, J. Quiroz, D.C. de Oliveira, P.H. Camargo, S.I. Córdoba de Torresi, In situ FTIR insights into the electrooxidation mechanism of glucose as a function of the surface facets of Cu_2O-based electrocatalytic sensors, J. Catal. 375 (2019) 95–103, http://dx.doi.org/10.1016/j.jcat.2019.05.032.

[14] K.E. Toghill, L. Xiao, M.A. Phillips, R.G. Compton, The non-enzymatic determination of glucose using an electrolytically fabricated nickel microparticle modified boron-doped diamond electrode or nickel foil electrode, Sensors Actuators, B: Chem. 147 (2010) 642–652, http://dx.doi.org/10.1016/j.snb.2010.03.091.

[15] T. Faverge, B. Gilles, A. Bonnefont, F. Maillard, C. Coutanceau, M. Chatenet, In situ investigation of D-glucose oxidation into value-added products on Au, Pt, and Pd under alkaline conditions: a comparative study, ACS Catal. 13 (2023) 2657–2669, http://dx.doi.org/10.1021/acscatal.2c05871.

[16] Y. Holade, K. Servat, T.W. Napporn, K.B. Kokoh, Selective nanomaterials for glucose-to-gluconate oxidation in an electrochemical energy converter: cogenerating organic electrosynthesis, ECS Trans. 77 (2017) 1547–1557, http://dx.doi.org/10.1149/07711.1547ecst.

[17] N. Schlegel, A. Bagger, J. Rossmeisl, M. Arenz, Elucidating the reaction pathway of glucose electrooxidation to its valuable products: the influence of mass transport and electrode potential on the product distribution, J. Phys. Chem. C 127 (2023) 18609–18618, http://dx.doi.org/10.1021/acs.jpcc.3c03055.

[18] A.J. Bard, L.R. Faulkner, Electrochemical Methods: Fundamentals and Applications, second ed., Wiley, 2001.

[19] I. Danaee, M. Jafarian, F. Forouzandeh, F. Gobal, Kinetic studies of glucose electrocatalytic oxidation on GC/Ni electrode, Int. J. Chem. Kinet. 44 (2012) 712–721, http://dx.doi.org/10.1002/kin.20721.

[20] A. Medrano-Banda, J. Guehl, G. Kéranguéven, A. Oshchepkov, E. Savinova, A. Bonnefont, Dual-path glucose electrooxidation reaction on $Ni(OH)_2$/NiOOH catalysts in alkaline media, Electrochim. Acta 476 (2024) 143692, http://dx.doi.org/10.1016/J.ELECTACTA.2023.143692.

[21] C. Zhao, C. Shao, M. Li, K. Jiao, Flow-injection analysis of glucose without enzyme based on electrocatalytic oxidation of glucose at a nickel electrode, Talanta 71 (2007) 1769–1773, http://dx.doi.org/10.1016/j.talanta.2006.08.013.

[22] G. Sanghez de Luna, T. Tabanelli, J.J. Velasco-Vélez, E. Monti, F. Ospitali, S. Albonetti, F. Cavani, G. Fornasari, P. Benito, Electrification of glucose valorization over NiO/Ni foam, Sustain. Energy Fuels 7 (2023) 4474–4485, http://dx.doi.org/10.1039/d3se00847a.

[23] L. Trotochaud, S.L. Young, J.K. Ranney, S.W. Boettcher, Nickel-Iron oxyhydroxide oxygen-evolution electrocatalysts: The role of intentional and incidental iron incorporation, J. Am. Chem. Soc. 136 (2014) 6744–6753, http://dx.doi.org/10.1021/ja502379c.

[24] A.G. Oshchepkov, G. Braesch, G. Rostamikia, A. Bonnefont, M.J. Janik, M. Chatenet, E.R. Savinova, Insights into the borohydride electrooxidation reaction on metallic nickel from operando FTIRS, on-line DEMS and DFT, Electrochim. Acta 389 (2021) 138721, http://dx.doi.org/10.1016/j.electacta.2021.138721.

[25] R.M. Tehrani, S. Ab Ghani, Electrocatalysis of free glycerol at a nanonickel modified graphite electrode and its determination in biodiesel, Electrochim. Acta 70 (2012) 153–157, http://dx.doi.org/10.1016/j.electacta.2012.03.044.

[26] N. Schlegel, G.K. Wiberg, M. Arenz, On the electrooxidation of glucose on gold: Towards an electrochemical glucaric acid production as value-added chemical, Electrochim. Acta 410 (2022) 140023, http://dx.doi.org/10.1016/j.electacta.2022.140023.

[27] E.G. Mahoney, W. Sheng, M. Cheng, K.X. Lee, Y. Yan, J.G. Chen, Analyzing the electrooxidation of ethylene glycol and glucose over platinum-modified gold electrocatalysts in alkaline electrolyte using in-situ infrared spectroscopy, J. Power Sources 305 (2016) 89–96, http://dx.doi.org/10.1016/j.jpowsour.2015.11.059.

[28] J.F. Gomes, A.C. Garcia, L.H. Gasparotto, N.E. De Souza, E.B. Ferreira, C. Pires, G. Tremiliosi-Filho, Influence of silver on the glycerol electro-oxidation over AuAg/C catalysts in alkaline medium: A cyclic voltammetry and in situ FTIR spectroscopy study, Electrochim. Acta 144 (2014) 361–368, http://dx.doi.org/10.1016/j.electacta.2014.08.035.

[29] V.M. Zemtsova, A.G. Oshchepkov, E.R. Savinova, Unveiling the role of iron in the nickel-catalyzed urea oxidation reaction, ACS Catal. 13 (2023) 13466–13473, http://dx.doi.org/10.1021/acscatal.3c03126.

[30] Y. Holade, A.B. Engel, K. Servat, T.W. Napporn, C. Morais, S. Tingry, D. Cornu, K.B. Kokoh, Electrocatalytic and electroanalytic investigation of carbohydrates oxidation on gold-based nanocatalysts in alkaline and neutral pHs, J. Electrochem. Soc. 165 (2018) H425–H436, http://dx.doi.org/10.1149/2.0311809jes.

[31] K. Ito, H.J. Bernstein, The vibrational spectra of the formate, acetate, and oxalate ions, Can. J. Chem. 34 (1956) 170–178, http://dx.doi.org/10.1139/v56-021.

[32] M. Tominaga, M. Nagashima, K. Nishiyama, I. Taniguchi, Surface poisoning during electrocatalytic monosaccharide oxidation reactions at gold electrodes in alkaline medium, Electrochem. Commun. 9 (2007) 1892–1898, http://dx.doi.org/10.1016/J.ELECOM.2007.04.024.

[33] E. Ginoux, G. Acosta, P. Cognet, Y. Pérès, L. Latapie, L. Estel, A. Ledoux, Preliminary study of electrochemical conversion of glucose on novel modified nickel electrodes, J. Appl. Electrochem. (2024) http://dx.doi.org/10.1007/s10800-024-02083-2.

[34] A. Hamelin, Z. Borowska, J. Stafiej, A double layer study of the (210) and (111) faces of gold in aqueous NaBF4 solutions, J. Electroanal. Chem. Interfacial Electrochem. 189 (1985) 85–97, http://dx.doi.org/10.1016/0368-1874(85)85627-6.

[35] A. Goyal, M.T. Koper, The interrelated effect of cations and electrolyte pH on the hydrogen evolution reaction on gold electrodes in alkaline media, Angew. Chem. Int. Edn 60 (2021) 13452–13462, http://dx.doi.org/10.1002/anie.202102803.

[36] S. Strbac, A. Hamelin, R.R. Adzić, Electrochemical indication of surface reconstruction of (100), (311) and (111) gold faces in alkaline solutions, J. Electroanal. Soc. 362 (1993) 47–53, http://dx.doi.org/10.1016/0022-0728(93)80005-3.

[37] A. Chen, J. Richer, S.G. Roscoe, J. Lipkowski, Electrochemical and Fourier transform infrared spectroscopy studies of benzonitrile adsorption at the Au(111) electrode, Langmuir 13 (1997) 4737–4747, http://dx.doi.org/10.1021/la9701586.

[38] V.L. Oliveira, C. Morais, K. Servat, T.W. Napporn, G. Tremiliosi-Filho, K.B. Kokoh, Glycerol oxidation on nickel based nanocatalysts in alkaline medium – Identification of the reaction products, J. Electroanal. Soc. 703 (2013) 56–62, http://dx.doi.org/10.1016/J.JELECHEM.2013.05.021.

[39] M.E. Ghaith, M.G. Abd El-Moghny, H.H. Alalawy, M.E. El-Shakre, M.S. El-Deab, Enhancing the performance of Ni nanoparticle modified carbon felt towards glycerol electrooxidation: impact of organic additive, RSC Adv. 13 (2023) 10893–10902, http://dx.doi.org/10.1039/D3RA01197F.

[40] W. Visscher, Ellipsometry of nickel-oxides and -hydroxides in alkaline electrolyte, Le J. de Phys. Colloques 44 (1983) 213–216, http://dx.doi.org/10.1051/JPHYSCOL:19831044.

[41] P.C. Laan, F.J. de Zwart, E.M. Wilson, A. Troglia, O.C. Lugier, N.J. Geels, R. Bliem, J.N. Reek, B. de Bruin, G. Rothenberg, N. Yan, Understanding the oxidative properties of nickel oxyhydroxide in alcohol oxidation reactions, ACS Catal. 13 (2023) 8467–8476, http://dx.doi.org/10.1021/acscatal.3c01120.

[42] W. Jud, C.A. Salazar, J. Imbrogno, J. Verghese, S.M. Guinness, J.N. Desrosiers, C.O. Kappe, D. Cantillo, Electrochemical oxidation of alcohols using nickel oxide hydroxide as heterogeneous electrocatalyst in batch and continuous flow, Org. Process Res. Dev. 26 (2022) 1486–1495, http://dx.doi.org/10.1021/acs.oprd.2c00064.

[43] V. Vedovato, K. Vanbroekhoven, D. Pant, J. Helsen, Electrosynthesis of biobased chemicals using carbohydrates as a feedstock, Molecules 25 (2020) 3712, http://dx.doi.org/10.3390/molecules25163712.

[44] Z. He, J. Hwang, Z. Gong, M. Zhou, N. Zhang, X. Kang, J.W. Han, Y. Chen, Promoting biomass electrooxidation via modulating proton and oxygen anion deintercalation in hydroxide, Nature Commun. 13 (2022) 3777, http://dx.doi.org/10.1038/s41467-022-31484-0.

[45] M. Kosmulski, Compilation of PZC and IEP of sparingly soluble metal oxides and hydroxides from literature, Adv. Colloid Interface Sci. 152 (2009) 14–25, http://dx.doi.org/10.1016/J.CIS.2009.08.003.

[46] Z. Gonzalez, B. Ferrari, A.J. Sanchez-Herencia, A. Caballero, J. Morales, Relevance of the semiconductor microstructure in the pseudocapacitance of the electrodes fabricated by EPD of binder-free β-$Ni(OH)_2$ nanoplatelets, J. Electrochem. Soc. 162 (2015) D3001–D3012, http://dx.doi.org/10.1149/2.0101511JES.

[47] L. Sironi, S. Rizzato, L. Lo Presti, Why is α-D-glucose monomorphic? Insights from accurate experimental charge density at 90 K, Cryst. Growth Des. 22 (2022) 6627–6638, http://dx.doi.org/10.1021/acs.cgd.2c00846.